

TimeMachine: A Time Series is Worth 4 Mambas for Long-term Forecasting

Md Atik Ahamed^{a,*} and Qiang Cheng^{a,b, **}

^aDepartment of Computer Science, University of Kentucky

^bInstitute for Biomedical Informatics, University of Kentucky

Abstract. Long-term time-series forecasting remains challenging due to the difficulty in capturing long-term dependencies, achieving linear scalability, and maintaining computational efficiency. We introduce TimeMachine, an innovative model that leverages Mamba, a state-space model, to capture long-term dependencies in multivariate time series data while maintaining linear scalability and small memory footprints. TimeMachine exploits the unique properties of time series data to produce salient contextual cues at multi-scales and leverage an innovative integrated quadruple-Mamba architecture to unify the handling of channel-mixing and channel-independence situations, thus enabling effective selection of contents for prediction against global and local contexts at different scales. Experimentally, TimeMachine achieves superior performance in prediction accuracy, scalability, and memory efficiency, as extensively validated using benchmark datasets.

Code availability: <https://github.com/Atik-Ahamed/TimeMachine>

1 Introduction

Long-term time-series forecasting (LTSF) is essential in various tasks across diverse fields, such as weather forecasting, anomaly detection, and resource planning in energy, agriculture, industry, and defense. Although numerous approaches have been developed for LTSF, they typically can achieve only one or two desired properties such as capturing long-term dependencies in multivariate time series (MTS), linear scalability in the amount of model parameters with respect to data, and computational efficiency or applicability in edge computing. It is still challenging to achieve these desirable properties simultaneously.

Capturing long-term dependencies, which are generally abundant in MTS data, is pivotal to LTSF. While linear models such as DLinera [33] and TiDE [6] achieve competitive performance with linear complexity and scalability, with accuracy on par with Transformer-based models, they usually rely on MLPs and linear projections that may not well capture long-range correlations [4]. Transformer-based models such as iTransformer [35], PatchTST [23], and Crossformer [35] have a strong ability to capture long-range dependencies and superior performance in LTSF accuracy, thanks to the self-attention mechanisms in Transformers [28]. However, they typically suffer from the quadratic complexity [6], limiting their scalability and applicability, e.g., in edge computing.

* Email: atikahamed@uky.edu

** Email: qiang.cheng@uky.edu, Corresponding Author.

Recently, state-space models (SSMs) [10, 11, 12, 13, 25] have emerged as powerful engines for sequence-based inference and have attracted growing research interest. These models are capable of inferring over very long sequences and exhibit distinctive properties, including the ability to capture long-range correlations with linear complexity and context-aware selectivity with hidden attention mechanisms [11, 2]. SSMs have demonstrated great potential in various domains, including genomics [11], tabular learning [1], graph data [3], and images [22], yet they remain unexplored for LTSF.

The under-utilization of SSMs in LTSF can be attributed to two main reasons. First, highly content- and context-selective SSMs have only been recently developed [11]. Second, and more importantly, effectively representing the context in time series data remains a challenge. Many Transformer-based models, such as Autoformer [29] and Informer [36], regard each time point as a token in a sequence, while more recent models like PatchTST [24] and iTransformer [21] leverage patches of the time series as tokens. However, our empirical experiments on real-world MTS data suggest that directly utilizing SSMs for LTSF by using either time points or patches as tokens could hardly achieve performance comparable to Transformer-based models. Considering the particular characteristics of MTS data, it is essential to extract more salient contextual cues tailored to SSMs.

MTS data typically have many channels with each variate corresponding to a channel. Many models, such as Informer [36], FEDformer [37], and Autoformer [29], handle MTS data to extract useful representations in a channel-mixing way, where the MTS input is treated as a two-dimensional matrix whose size is the number of channels multiplied by the length of history. Nonetheless, recently a few works such as PatchTST [23] and TiDE [6] have shown that a channel-independence way for handling MTS may achieve SOTA accuracy, where each channel is input to the model as a one-dimensional vector independent of the other channels. We believe that these two ways of handling LTSF need to be adopted as per the characteristics of the MTS data, rather than using a one-size-fits-all approach. When there are strong between-channel correlations, channel mixing usually can help capture such dependencies; otherwise, channel independence is a more sensible choice. Therefore, it is necessary to design a unified architecture applicable to both channel-mixing and channel-independence scenarios.

Moreover, time series data exhibit a unique property – Temporal relations are largely preserved after downsampling into two subsequences. Few methods such as Scinet [19] have explored this property in designing their models; however, it is under-utilized in other approaches. Due to the high redundancy of MTS values at consecu-

tive time points, directly using time points as tokens may have redundant values obscure context-based selection and, more importantly, overlook long-range dependencies. Rather than relying on individual time points, using patches may provide contextual clues within each time window of a patch length. However, a pre-defined small patch length only provides contexts at a fixed temporal or frequency resolution, whereas long-range contexts may span different patches. To best capture long-range dependencies, it is sensible to supply multi-scale contexts and, at each scale, automatically produce global-level tokens as contexts similar to iTransformer [21] that tokenizes the whole look-back window. Further, while models like Transformer and the selective SSMs [11] have the ability to select sub-token contents, such ability is limited in the channel-independence case, for which local contexts need to be enhanced when leveraging SSMs for LTSF.

In this paper, we introduce a novel approach that effectively captures long-range dependencies in time series data by providing sensible multi-scale contexts and particularly enhancing local contexts in the channel-independence situation. Our model, built upon a selective scan SSM called Mamba [11], serves as a core inference engine with a strong ability to capture long-range dependencies in MTS data while maintaining linear scalability and small memory footprints. The proposed model exploits the unique property of time series data in a bottom-up manner by producing contextual cues at two scales through consecutive resolution reduction or downsampling using linear mapping. The first level operates at a high resolution, while the second level works at a low resolution. At each level, we employ two Mamba modules to glean contextual cues from global perspectives for the channel-mixing case and from both global and local perspectives for the channel-independence case.

In summary, our major contributions are threefold:

- We develop an innovative model called TimeMachine that is the first to leverage purely SSM modules to capture long-term dependencies in multivariate time series data for context-aware prediction, with linear scalability and small memory footprints superior or comparable to linear models.
- Our model constitutes an innovative architecture that unifies the handling of channel-mixing and channel-independence situations with four SSM modules, exploiting potential between-channel correlations. Moreover, our model can effectively select contents for prediction against global and local contextual information, at different scales in the MTS data.
- Experimentally, TimeMachine achieves superior performance in prediction accuracy, scalability, and memory efficiency. We extensively validate the model using standard benchmark datasets and perform rigorous ablation studies to demonstrate its effectiveness.

2 Related Works

Numerous methods for LTSF have been proposed, which can be grouped into three main categories: non-Transformer-based supervised approaches, Transformer-based supervised learning models, and self-supervised representation learning models.

Non-Transformer-based Supervised Approaches include classical methods like ARIMA, VARMAX, GARCH [5], and RNN [15], as well as deep learning-based methods that achieve state-of-the-art (SOTA) performance using multi-layer perceptrons (MLPs) and convolutional neural networks (CNNs). MLP-based models, such as DLinear [33], TiDE [6], and RLinear [18], leverage the simplicity of linear structures to achieve complexity and scalability.

CNN-based methods, such as TimesNet [30] and Scinet [19], utilize convolutional filters to extract valuable temporal features and model complex temporal dynamics. These approaches exhibit highly competitive performance, often comparable to or even occasionally outperforming more sophisticated Transformer-based models.

Transformer-based Supervised Learning Methods, such as iTransformer [21], PatchTST [23], Crossformer [35], FEDformer [37], stationary [20], and autoformer [29], have gained popularity for LTSF due to their superior accuracy. These methods convert time series to token sequences and leverage the self-attention mechanism to discover dependencies between arbitrary time steps, making them particularly effective for modeling complex temporal relationships. They may also exploit Transformers' ability to process data in parallel, enabling long-term dependency discovery sometimes with even linear scalability. Despite their distinctive advantages, these methods typically have quadratic time and memory complexity due to point-wise correlations in self-attention mechanisms.

Self-Supervised Representation Learning Models: Self-supervised learning has been leveraged to learn useful representations of MTS for downstream tasks, using non-Transformer-based models for time series [31, 9, 26, 32], and Transformer-based models such as time series Transformer (TST) and TS-TCC [34, 7, 27]. Currently, Transformer-based self-supervised models have not yet achieved performance on par with supervised learning approaches [27]. This paper focuses on LTSF in a supervised learning setting.

3 Proposed Method

In this section, we describe each component of our proposed architecture and how we use our model to solve the LTSF problem. Assume a collection of MTS samples is given, denoted by dataset \mathcal{D} , which comprises an input sequence $x = [x_1, \dots, x_L]$, with each $x_t \in \mathcal{R}^M$ representing a vector of M measurements at time point t . The sequence length L is also known as the look-back window. The goal is to predict T future values, denoted by $[x_{L+1}, \dots, x_{L+T}]$. The architecture of our proposed model, referred to as TimeMachine, is depicted in Figure 1. The pillars of this architecture consist of four Mambas, which are employed in an integrated way to tap contextual cues from MTS. This design choice enables us to harness Mamba's robust capabilities of inferring sequential data for LTSF.

Normalization: Before feeding the data to our model, we normalize the original MTS x into $x^0 = [x_1^{(0)}, \dots, x_L^{(0)}] \in \mathcal{R}^{M \times L}$, via $x^{(0)} = \text{Normalize}(x)$. Here, $\text{Normalize}(\cdot)$ represents a normalization operation with two different options. The first is to use the reversible instance normalization (RevIN) [16], which is also adopted in PatchTST [23]. The second option is to employ regular Z -score normalization: $x_{i,j}^{(0)} = (x_{i,j} - \text{mean}(x_{i,j})) / \sigma_j$, where σ_j is the standard deviation for channel j , with $j = 1, \dots, M$. Empirically we find that RevIN is often more helpful compared to Z -score. Apart from normalizing the data in the forward pass of our approach, in experiments, we also follow the standardization process of the data when compared with baseline methods.

Channel Mixing vs. Channel Independence: Our model can handle both channel independence and channel mixing cases. In channel independence, each channel is processed independently by our model, while in channel mixing, the MTS sequence is processed with multiple channels combined throughout our architecture. Regardless of the case, our model accepts input of the shape BML and produces

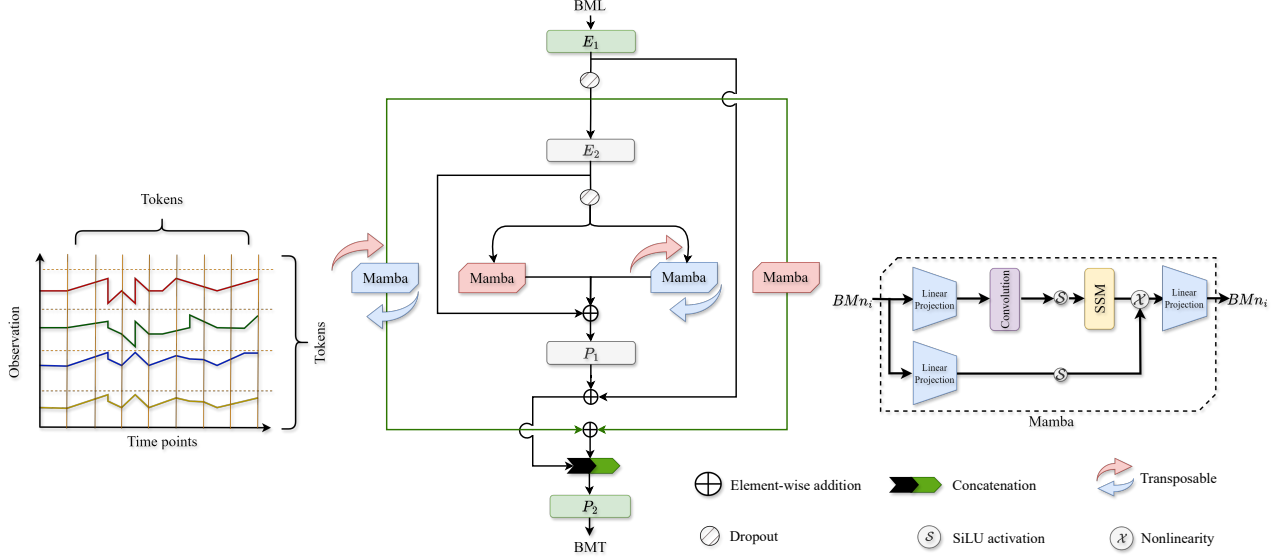


Figure 1: Schematic diagram of our proposed methodology, TimeMachine. Our method incorporates a configuration of four Mambas, with two specialized Mambas capable of processing the transposed signal data in each branch. To the left, an example of the TimeSeries signals is depicted, while the right side offers a detailed zoomed-in view of a Mamba’s structure. Mambas are capable of accepting an input of shape BMn_i while providing the same shape as the output. In our method $i \in \{1, 2\}$.

the desired output of the shape BMT , eliminating the need for additional manual pre-processing.

Channel independence has been proven effective in reducing overfitting by PatchTST [23]. We found this strategy helpful for datasets with a smaller number of channels. However, for datasets with a number of channels comparable to the look-back, channel mixing is more effective in capturing the correlations among channels and reaching the desired minimum loss during training.

Our architecture is robust and versatile, capable of benefiting from potentially strong inter-channel correlations in channel-mixing case and exploiting independence in channel-independence case. When dealing with channel independence, we reshape the input from BML to $(B \times M)1L$ after the normalization step. The reshaped input is then processed throughout the network and later merged to provide an output shape of BMT . In contrast, for channel mixing, no reshaping is necessary. The channels are kept together and processed throughout the network.

Embedded Representations: Before processing the input sequence with Mambas, we provide two-stage embedded representations of the input sequence with length L by E_1 and E_2 :

$$x^{(1)} = E_1(x^{(0)}), \quad x^{(2)} = E_2(DO(x^{(1)})), \quad (1)$$

where DO stands for the dropout operation, and the embedding operations $E_1 : \mathbb{R}^{M \times L} \rightarrow \mathbb{R}^{M \times n_1}$ and $E_2 : \mathbb{R}^{M \times n_1} \rightarrow \mathbb{R}^{M \times n_2}$ are achieved through MLPs. Thus, for the channel mixing case, the batch-formed tensors will have the following changes in size: $BMn_1 \leftarrow E_1(BML)$, and $BMn_2 \leftarrow E_2(BMn_1)$. This enables us to deal with the fixed-length tokens of n_1 and n_2 regardless of the variable input sequence length L , and both n_1 and n_2 are configured to take values from the set $\{512, 256, 128, 64, 32\}$ satisfying $n_1 > n_2$. Since MLPs are fully connected, we introduce dropouts to reduce overfitting. Although we have the linear mappings (MLPs) before Mambas, the performance of our model does not heavily rely on them, as demonstrated with the ablation study (see Section 5).

Integrated Quadruple Mambas: With the two processed embedded representations from E_1 , E_2 , we can now learn more comprehensive representations by leveraging Mamba, a type of SSM with selective scan ability. At each embedding level, we employ a pair of Mambas to capture long-term dependencies within the look-back samples and provide sufficient local contexts. Denote the input to one of the four Mamba blocks by u , which is either $DO(x^{(1)})$ obtained after E_1 and the subsequent dropout layer for the two outer Mambas, or $DO(x^{(2)})$ obtained after E_2 and the subsequent dropout layer for the two inner Mambas (Figure 1). The input tensors may be reshaped per channel mixing or channel independence cases as described previously.

Inside a Mamba block, two fully-connected layers in two branches calculate linear projections. The output of the linear mapping in the first branch passes through a 1D causal convolution and SiLU activation $\mathcal{S}(\cdot)$ [8], then a structured SSM. The continuous-time SSM maps an input function or sequence $u(t)$ to output $v(t)$ through a latent state $h(t)$:

$$dh(t)/dt = A h(t) + B u(t), \quad v(t) = C h(t), \quad (2)$$

where $h(t)$ is N -dimensional, with N also known as a state expansion factor, $u(t)$ is D -dimensional, with D being the dimension factor for an input token, $v(t)$ is an output of dimension D , and A , B , and C are coefficient matrices of proper sizes. This dynamic system induces a discrete SSM governing state evolution and outputs given the input token sequence through time sampling at $\{k\Delta\}$ with a Δ time interval. This discrete SSM is

$$h_k = \bar{A} h_{k-1} + \bar{B} u_k, \quad v_k = C h_k, \quad (3)$$

where h_k , u_k , and v_k are respectively samples of $h(t)$, $u(t)$, and $v(t)$ at time $k\Delta$,

$$\bar{A} = \exp(\Delta A), \quad \bar{B} = (\Delta A)^{-1}(\exp(\Delta A) - I)\Delta B. \quad (4)$$

For SSMs, diagonal A is often used. Mamba makes B , C , and Δ linear time-varying functions dependent on the input. In particular, for a

token $u, B, C \leftarrow \text{Linear}_N(u)$, and $\Delta \leftarrow \text{softplus}(\text{parameter} + \text{Linear}_D(\text{Linear}_1(u)))$, where $\text{Linear}_p(u)$ is a linear projection to a p -dimensional space, and softplus activation function. Furthermore, Mamba also has an option to expand the model dimension factor D by a controllable dimension expansion factor E . Such coefficient matrices enable context and input selectivity properties [11] to selectively propagate or forget information along the input token sequence based on the current token. Subsequently, the SSM output is multiplicatively modulated with the output from the second branch before another fully connected projection. The second branch simply consists of a linear mapping followed by a SiLU.

Processed embedded representation with tensor size BMn_1 is transformed by outer Mambas, while that with BMn_2 is transformed by inner Mambas, as depicted in Figure 1. For the channel-mixing case, the whole univariate sequence of each channel is used as a token with dimension factor n_2 for the inner Mambas. The outputs from the left-side and right-side inner Mambas, $v_{L,k}, v_{R,k} \in \mathcal{R}^{n_2}$, are element-wise added with $x_k^{(2)}$ to obtain $x_k^{(3)}$ for the k -th token, $k = 1, \dots, M$. That is, by denoting $v_L = [v_{L,1}, \dots, v_{L,M}] \in \mathcal{R}^{M \times n_2}$ and similarly $v_R \in \mathcal{R}^{M \times n_2}$, we have $x^{(3)} = v_L \oplus v_R \oplus x^{(2)}$, with \oplus being element-wise addition. Then, $x^{(3)}$ is linearly mapped to $x^{(4)}$ with $P_1 : x^{(3)} \rightarrow x^{(4)} \in \mathcal{R}^{M \times n_1}$. Similarly, the outputs from the outer Mambas, $v_{L,k}^*, v_{R,k}^* \in \mathcal{R}^{n_1}$ are element-wise added to obtain $x^{(5)} \in \mathcal{R}^{M \times n_1}$.

For the channel independence case, the input is reshaped, $BML \mapsto (B \times M)1L$, and the embedded representations become $(B \times M)1n_1$ and $(B \times M)1n_2$. One Mamba in each pair of outer Mambas or inner Mambas considers the input dimension as 1 and the token length as n_1 or n_2 , while the other Mamba learns with input dimension n_2 or n_1 and token length 1. This design enables learning both global context and local context simultaneously. The outer and inner pairs of Mambas will extract salient features and context cues are fine and coarse scales with high- and low-resolution, respectively.

Channel mixing is performed when the datasets contain a significantly large number of channels, in particular, when the look-back L is comparable to the channel number M , taking the whole sequence as a token to better provide context cues. All four Mambas are used to capture the global context of the sequences at different scales and learn from the channel correlations. This helps stabilize the training and reduce overfitting with large M . To switch between the channel-independence and channel-mixing cases, the input sequence is simply transposed, with one Mamba in each branch processing the transposed input, as demonstrated in Figure 1.

These integrated Mamba blocks empower our model for content-dependent feature extraction and reasoning with long-range dependencies and feature interactions.

Output Projection: After receiving the output tokens from the Mambas, our goal is to project these tokens to generate predictions with the desired sequence length. To accomplish this task, we utilize two MLPs, P_1 and P_2 , which output n_1 and T time points, respectively, with each point having M channels. Specifically, projector P_1 performs a mapping $\mathcal{R}^{M \times n_2} \rightarrow \mathcal{R}^{M \times n_1}$, as discussed above for obtaining $x^{(4)}$. Subsequently, projector P_2 performs a mapping $\mathbb{R}^{M \times 2n_1} \rightarrow \mathbb{R}^{M \times T}$, transforming the concatenated output from the Mambas into the final predictions. The use of a two-stage output projection via P_1 and P_2 symmetrically aligns with the two-stage embedded representation obtained through E_1 and E_2 .

In addition to the token transformation, we also employ residual connections. One residual connection is added before P_1 , and another is added after P_1 . The effectiveness of these residual connec-

Table 1: Overview of the characteristics of used benchmarking datasets. Time points illustrate the total length of each dataset

Dataset (\mathcal{D})	Channels (M)	Time Points	Frequency
Weather	21	52696	10 Minutes
Traffic	862	17544	Hourly
Electricity	321	26304	Hourly
ETTh1	7	17420	Hourly
ETTh2	7	17420	Hourly
ETTm1	7	69680	15 Minutes
ETTm2	7	69680	15 Minutes

tions is verified by experimental results (see Supplementary Table 1). Residual connections are demonstrated by arrows and element-wise addition in our method (Figure 1).

To retain the information of both outer and inner pairs of Mambas we concatenate their representations before processing via P_2 . In summary, we concatenate the outputs of the four Mambas with a skip connection to have $x^{(6)} = x^{(5)} \parallel (x^{(4)} \oplus x^{(1)})$, where \parallel denotes concatenation. Finally, the output y is obtained by applying P_2 to $x^{(6)}$, i.e., $y = P_2(x^{(6)})$.

4 Result Analysis

In this segment, we present the main results of our experiments on widely recognized benchmark datasets for long-term MTS forecasting. We also conduct extensive ablation studies to demonstrate the effectiveness of each component of our method.

4.1 Datasets

We evaluate our model on seven benchmark datasets extensively used for LTSF: Weather, Traffic, Electricity, and four ETT datasets (ETTh1, ETTh2, ETTm1, ETTm2). Table 1 illustrates the relevant statistics of these datasets, highlighting that the Traffic and Electricity datasets notably large, with 862 and 321 channels, respectively, and tens of thousands of temporal points in each sequence. More details on these datasets can be found in Wu et al. [29], Zhou et al. [36]. Focusing on long-term forecasting, we exclude the ILI dataset, which has a shorter temporal horizon, similar to Das et al. [6]. We demonstrate the superiority of our model in two parts: quantitative (main results) and qualitative results. For a fair comparison, we used the code from PatchTST [23]¹ and iTransformer [21]², and we took the results for the baseline methods from iTransformer [21].

4.2 Experimental Environment

All experiments were conducted using the PyTorch framework [24] with NVIDIA 4XV100 GPUs (32GB each). The model was optimized using the ADAM algorithm [17] with L_2 loss. The batch size varied depending on the dataset, but the training was consistently set to 100 epochs. We measure the prediction errors using mean square error (MSE) and mean absolute error (MAE) metrics, where smaller values indicate better prediction accuracy.

Baseline Models: We compared our model, TimeMachine, with 11 SOTA models, including iTransformer [21], PatchTST [23], DLinear [33], RLinear [18], Autoformer [29], Crossformer [35], TiDE [6], Scinet [19], TimesNet [30], FEDformer [37], and Stationary [20]. Although another variant of SSMs, namely S4 [12], exists,

¹ <https://github.com/yuqinie98/PatchTST>

² <https://github.com/thuml/iTransformer>

we do not include it in our comparison because TiDE [6] has already demonstrated superior performance over S4.

4.3 Quantitative Results

We demonstrate TimeMachine’s performance in supervised long-term forecasting tasks in Table 2. Following the protocol used in iTransformer [21], we set all baselines fixed with $L = 96$ and $T = \{96, 192, 336, 720\}$, including our method. For all results achieved by our model, we utilized the training-related values mentioned in Section 4. In addition to the training hyperparameters, we set default values for all Mambas: Dimension factor $D = 256$, local convolutional width = 2, and state expand factor $N = 1$. We provide an experimental justification for these parameters in Section 5. Table 2 clearly shows that our method demonstrates superior performance compared to all the strong baselines in almost all datasets. Moreover, iTransformer [21] has significantly better performance than other baselines on the Traffic and Electricity datasets, which contain a large number of channels. Our method also demonstrates comparable or superior performance on these two datasets, outperforming the existing strong baselines by a large margin. This demonstrates the effectiveness of our method in handling LTSF tasks with varying number of channels and datasets.

In addition to Table 2, we conducted experiments with TimeMachine using different look-back windows $L = \{192, 336, 720\}$. Table 3 and Supplementary Table 2 demonstrate TimeMachine’s performance under these settings. An examination of these tables reveals that the implementation of extended look-back windows markedly enhances the performance of our method across the majority of the datasets examined. This also demonstrates TimeMachine’s capability for handling longer look-back windows while maintaining consistent performance.

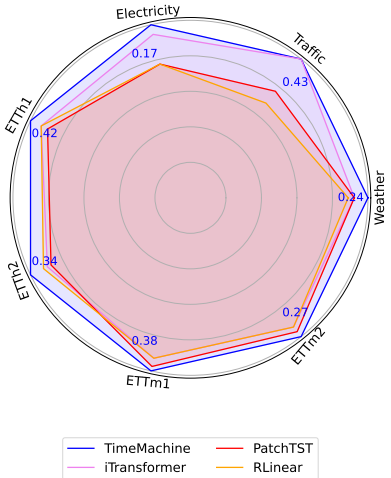


Figure 2: Average performance (in MSE) comparison among TimeMachine and the latest SOTA baselines with input sequence length $L = 96$. The center of the circle represents the maximum possible error. The closer to the boundary, the better the performance.

Following iTransformer [21], Figure 2 demonstrates the normalized percentage gain of TimeMachine with respect to three other SOTA methods, indicating a clear improvement over the strong baselines. In addition to general performance comparison using MSE and MAE metrics, we also compare the memory footprints and scalability of our method against other baselines in Figure 4. We measured the GPU memory utilization of our method and compared it against other baselines, with results for other baseline models taken from the

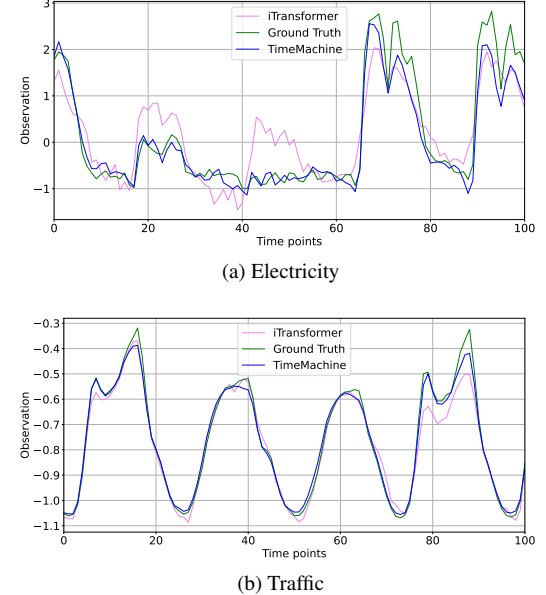


Figure 3: Qualitative comparison between TimeMachine and second-best-performing methods from Table 2. Observations are demonstrated from the test set for the case of $L = 96$ and $T = 720$ with a randomly selected channel and window frame of 100 time points. iTransformer [21] paper. To ensure a fair comparison, we set the experimental settings for our method similar to those of iTransformer.

The results clearly show very small memory footprints compared to SOTA baselines. Specifically for Traffic, our method consumes a very similar amount of memory to the DLinear [33] method. Moreover, our method is capable of handling longer look-back windows with a relatively linear increase in the number of learnable parameters, as demonstrated in Supplementary Figure 4 for two datasets. This is due to the robustness of our method, where E_1 is only dependent on the input sequence length L , and the rest of the networks are relatively independent of L , leading to a highly scalable model.

4.4 Qualitative Results

Figure 3 and supplementary Figure 2 demonstrate TimeMachine’s effectiveness in visual comparison. It is evident that TimeMachine can follow the actual trend in the predicted future time horizon for the test set. In the case of the Electricity dataset, there is a clear difference between the performance of TimeMachine and iTransformer. For the Traffic dataset, although both iTransformer and Timemachine’s performance align with the ground truth, in the range approximately between 75-90, TimeMachine’s performance is more closely aligned with the ground truth compared to iTransformer. For better visualization, we demonstrated a window of 100 predicted time points.

5 Hyperparameter Sensitivity Analysis and Ablation Study

In this section, we conducted experiments on various hyperparameters, including training and method-specific parameters. For each parameter, we provided experimental justification based on the achieved results. While conducting an ablation experiment on a parameter, other parameters were kept fixed at their default values, ensuring a clear justification for that specific parameter.

Table 2: Results in MSE and MAE (the lower the better) for the long-term forecasting task. We compare extensively with baselines under different prediction lengths, $T = \{96, 192, 336, 720\}$ following the setting of iTransformer [21]. The length of the input sequence (L) is set to 96 for all baselines. The best results are in **bold** and the second best are underlined.

Methods →		TimeMachine		iTransformer		RLinear		PatchTST		Crossformer		TiDE		TimesNet		DLinear		SCINet		FEDformer		Stationary		Autoformer	
\mathcal{D}	T	MSE	MAE	MSE	MAE	MSE	MAE	MSE	MAE	MSE	MAE	MSE	MAE	MSE	MAE	MSE	MAE								
Weather	96	0.164	0.208	0.174	0.214	0.192	0.232	0.177	0.218	0.158	0.230	0.202	0.261	0.172	0.220	0.196	0.255	0.221	0.306	0.217	0.296	0.173	0.223	0.266	0.336
	192	<u>0.211</u>	0.250	0.221	<u>0.254</u>	0.240	0.271	0.225	0.259	0.206	0.277	0.242	0.298	0.219	0.261	0.237	0.296	0.261	0.340	0.276	0.336	0.245	0.285	0.307	0.367
	336	0.256	0.290	0.278	0.296	0.292	0.307	0.278	0.297	<u>0.272</u>	0.335	0.287	0.335	0.280	0.306	0.283	0.335	0.309	0.378	0.339	0.380	0.321	0.338	0.359	0.395
	720	0.342	0.343	0.358	<u>0.349</u>	0.364	0.353	0.354	0.348	0.398	0.418	<u>0.351</u>	0.386	0.365	0.359	0.345	0.381	0.377	0.427	0.403	0.428	0.414	0.410	0.419	0.428
Traffic	96	<u>0.397</u>	0.268	0.395	0.268	0.649	0.389	0.544	0.359	0.522	<u>0.290</u>	0.805	0.493	0.593	0.321	0.650	0.396	0.788	0.499	0.587	0.366	0.612	0.338	0.613	0.388
	192	0.417	0.274	0.417	<u>0.276</u>	0.601	0.366	0.540	0.354	<u>0.530</u>	0.293	0.756	0.474	0.617	0.336	0.598	0.370	0.789	0.505	0.604	0.373	0.613	0.340	0.616	0.382
	336	0.433	0.281	0.433	<u>0.283</u>	0.609	0.369	<u>0.551</u>	0.358	0.558	0.305	0.762	0.477	0.629	0.336	0.605	0.373	0.797	0.508	0.621	0.383	0.618	0.328	0.622	0.337
	720	0.467	0.300	<u>0.467</u>	<u>0.302</u>	0.647	0.387	<u>0.586</u>	0.375	0.589	0.328	0.719	0.449	0.640	0.350	<u>0.645</u>	0.394	0.841	0.523	0.626	0.382	0.653	0.355	0.660	0.408
Electricity	96	0.142	0.236	0.148	0.240	0.201	0.281	0.195	0.285	0.219	0.314	0.237	0.329	0.168	0.272	0.197	0.282	0.247	0.345	0.193	0.308	0.169	0.273	0.201	0.317
	192	0.158	0.250	0.162	<u>0.253</u>	0.201	0.283	0.199	0.289	0.231	0.322	0.236	0.330	0.184	0.289	0.196	0.285	0.257	0.355	0.201	0.315	0.182	0.286	0.222	0.334
	336	0.172	0.268	0.178	0.269	0.215	0.298	0.215	0.305	0.246	0.337	0.249	0.344	0.198	0.300	0.209	0.301	0.269	0.369	0.214	0.329	0.200	0.304	0.231	0.338
	720	0.207	0.298	0.225	<u>0.317</u>	0.257	0.331	0.256	0.337	0.280	0.363	0.284	0.373	0.220	0.320	0.245	0.333	0.299	0.390	0.246	0.355	0.222	0.321	0.254	0.361
ETTh1	96	0.364	0.387	0.386	0.405	0.386	0.395	0.414	0.419	0.423	0.448	0.479	0.464	0.384	0.402	0.386	0.400	0.654	0.599	0.376	0.419	0.513	0.491	0.449	0.459
	192	0.415	0.416	0.441	0.436	0.437	<u>0.424</u>	0.460	0.445	0.471	0.474	0.525	0.492	0.436	0.429	0.437	0.432	0.719	0.631	0.420	0.448	0.534	0.504	0.500	0.482
	336	0.429	0.421	0.487	0.458	0.479	<u>0.446</u>	0.501	0.466	0.570	0.546	0.565	0.515	0.491	0.469	0.481	0.459	0.778	0.659	0.459	0.465	0.588	0.535	0.521	0.496
	720	0.458	0.453	0.503	0.491	0.481	0.470	0.500	0.488	0.653	0.621	0.594	0.558	0.521	0.500	0.519	0.516	0.836	0.699	0.506	0.507	0.643	0.616	0.514	0.512
ETTh2	96	0.275	0.334	0.297	0.349	0.288	<u>0.338</u>	0.302	0.348	0.745	0.584	0.400	0.440	0.340	0.374	0.333	0.387	0.707	0.621	0.358	0.397	0.476	0.458	0.346	0.388
	192	0.349	0.381	0.380	0.400	<u>0.374</u>	<u>0.390</u>	0.388	0.400	0.877	0.656	0.528	0.509	0.402	0.414	0.477	0.476	0.860	0.689	0.429	0.439	0.512	0.493	0.456	0.452
	336	0.340	0.381	0.428	0.432	<u>0.415</u>	<u>0.426</u>	0.426	0.433	1.043	0.731	0.643	0.571	0.452	0.452	0.594	0.541	1.000	0.744	0.496	0.487	0.552	0.551	0.482	0.486
	720	0.411	0.433	0.427	0.445	<u>0.420</u>	<u>0.440</u>	0.431	0.446	1.104	0.763	0.874	0.679	0.462	0.468	0.831	0.657	1.249	0.838	0.463	0.474	0.562	0.560	0.515	0.511
ETTm1	96	0.317	0.355	0.334	0.368	0.355	0.376	0.329	0.367	0.404	0.426	0.364	0.387	0.338	0.375	0.345	0.372	0.418	0.438	0.379	0.419	0.386	0.398	0.505	0.475
	192	0.357	0.378	0.377	0.391	0.391	0.392	<u>0.367</u>	<u>0.385</u>	0.450	0.451	0.398	0.404	0.374	0.387	0.380	0.389	0.439	0.450	0.426	0.441	0.459	0.444	0.553	0.496
	336	0.379	0.399	0.426	0.420	0.424	0.415	0.399	0.410	0.532	0.515	0.428	0.425	0.410	0.411	0.413	0.413	0.490	0.485	0.445	0.459	0.495	0.464	0.621	0.537
	720	0.445	0.436	0.491	0.459	0.487	0.450	<u>0.454</u>	<u>0.439</u>	0.666	0.589	0.487	0.461	0.478	0.450	0.474	0.453	0.595	0.550	0.543	0.490	0.585	0.516	0.671	0.561
ETTm2	96	0.175	0.256	0.180	0.264	0.182	<u>0.265</u>	0.175	<u>0.259</u>	0.287	0.366	0.207	0.305	0.187	0.267	0.193	0.292	0.286	0.377	0.203	0.287	0.192	0.274	0.255	0.339
	192	0.239	0.299	0.250	0.309	0.246	0.304	<u>0.241</u>	<u>0.302</u>	0.414	0.492	0.290	0.364	0.249	0.309	0.284	0.362	0.399	0.445	0.269	0.328	0.280	0.339	0.281	0.340
	336	0.287	0.332	0.311	0.348	0.307	<u>0.342</u>	<u>0.305</u>	0.343	0.597	0.542	0.377	0.422	0.321	0.351	0.369	0.427	0.637	0.591	0.325	0.366	0.334	0.361	0.339	0.372
	720	0.371	0.385	0.412	0.407	0.407	<u>0.398</u>	<u>0.402</u>	0.400	1.730	1.042	0.558	0.524	0.408	0.403	0.554	0.522	0.960	0.735	0.421	0.415	0.417	0.413	0.433	0.432

Table 3: Results for the long-term forecasting task with varying $L = \{192, 336, 720\}$ and $T = \{96, 192, 336, 720\}$

Prediction (T) →		96	192	336	720
\mathcal{D}	L	MSE	MAE	MSE	MAE
Traffic	192	0.362	0.252	0.386	0.262
	336	0.355	0.249	0.378	0.259
	720	0.348	0.249	0.364	0.255
Elec.	192	0.135	0.230	0.167	0.258
	336	0.133	0.225	0.160	0.255
	720	0.133	0.225	0.160	0.257
ETTm2	192	0.170	0.252	0.230	0.294
	336	0.165	0.254	0.223	0.291
	720	0.163	0.253	0.222	0.295

5.1 Effect of MLPs' Parameters (n_1, n_2)

As demonstrated in Figure 1, we have two stages of compression with two MLPs E_1, E_2 of output dimensions n_1 and n_2 , respectively, and P_1 performing an expansion by converting $n_2 \rightarrow n_1$. Since several strong baseline methods, e.g., DLinear, leverage mainly MLPs, we aim at understanding the effect of MLPs on performance. To this end, we explored 10 different combinations from $\{512, 256, 128, 64, 32\}$ and demonstrated the performance with MSE for two datasets (ETTh1, ETTh2) in Figure 5. These figures show that our method is not heavily dependent on the MLPs. Rather, we can see more improvement with very small MLPs for $T = 720$ with the ETTh1 dataset and mostly stable performance on the ETTh2 dataset.

5.2 Sensitivity of Dropouts

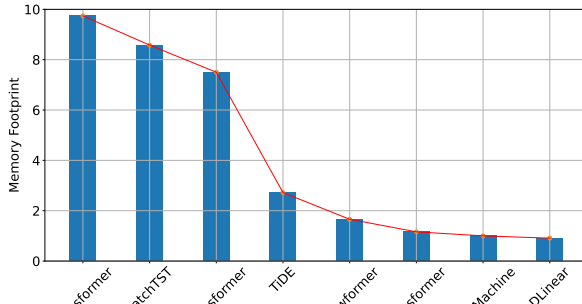
In our model (Figure 1), we include two dropouts after processing the signals from E_1 and E_2 . These dropouts are necessary, especially for datasets with a small number of channels, e.g., ETThs. Supplementary Figure 1 shows the effect of dropouts on both ETTh1 and ETTh2 datasets. As expected, too low or too high dropout rates are not helpful. To maintain balance, we set the dropout rates to 0.7 for both datasets while tuning other variations for the rest.

5.3 Ablation of Residual Connections

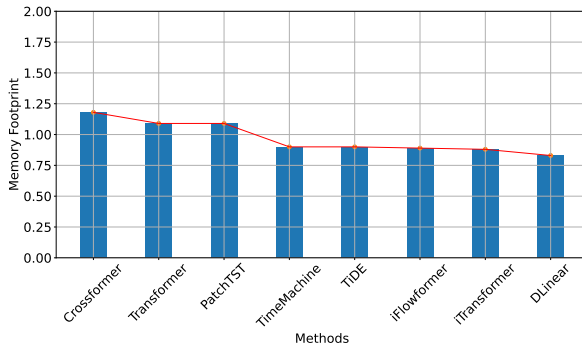
Studies have shown the effectiveness of residual connection, including models using SSMs [1] and CNNs [14]. In this section, we justify the two residual connections in our architecture: one from E_2 to the output of the two inner Mambas, and the other from E_1 to the output of P_1 . These residual connections help stabilize training and reduce overfitting, especially for the smaller datasets with channel independence. Supplementary Table 1 provides experimental justification, where the Res. column indicates the presence (✓) or absence (✗) of residual connections. We observe clear improvement on both datasets when residual connections are used. This motivated us to include residual connections in our architecture, and all results presented in Tables 2 and 3 incorporate these connections.

5.4 Effects of Mambas' Local Convolutional Width

In addition to experimenting with the different components of our architecture (Figure 1), we also investigated the effectiveness of Mamba parameters. For example, we tested two variations of local convolutional kernel widths (2 and 4) for the Mambas and found that a kernel width of 2 yields more promising results compared to 4.

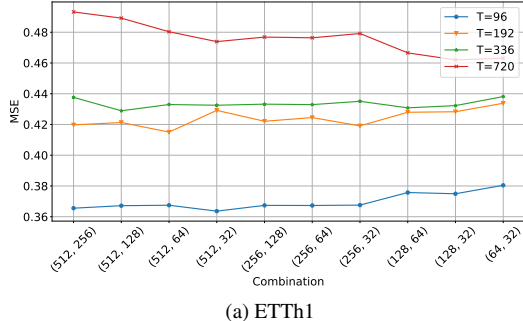


(a) Traffic

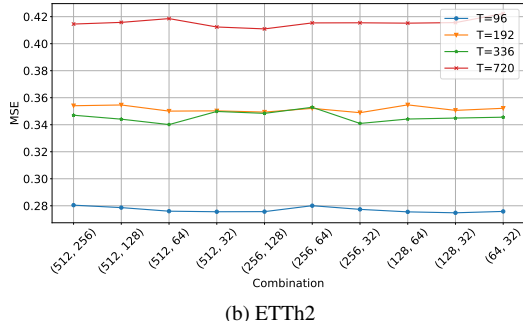


(b) Weather

Figure 4: Memory footprint (in GB) for Traffic (with 862 channels) and Weather (with 21 channels) following iTransformer [21].



(a) ETTh1



(b) ETTh2

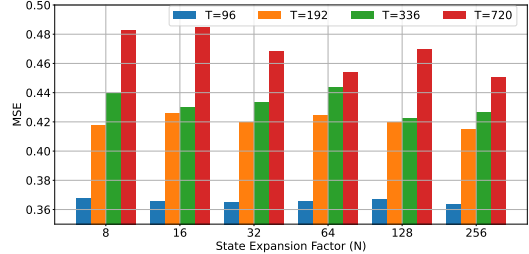
Figure 5: MSE comparison with combinations of n_1 and n_2 for input sequence length $L = 96$ for the ETTh1 and ETTh2 datasets. Therefore, we set the default kernel width to 2 for all datasets and Mambas.

5.5 Ablation on State Expansion Factor of Mambas

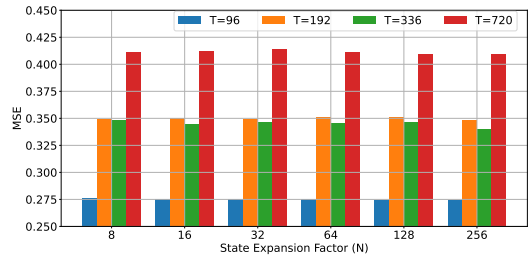
The SSM state expansion factor (N) is another crucial parameter of Mamba. We ablate this parameter from a very small value of 8 up to

Table 4: Ablation experiment on the local convolution width with input sequence length $L = 96$.

Prediction (T) →		96		192		336		720	
\mathcal{D}	d_{conv}	MSE	MAE	MSE	MAE	MSE	MAE	MSE	MAE
ETTh1	4	0.365	0.389	0.419	0.418	0.439	0.424	0.465	0.457
	2	0.364	0.387	0.415	0.416	0.429	0.421	0.458	0.453
ETTh2	4	0.275	0.333	0.347	0.383	0.350	0.382	0.411	0.433
	2	0.275	0.334	0.349	0.381	0.340	0.381	0.411	0.433



(a) ETTh1



(b) ETTh2

Figure 6: MSE versus the state expansion factor (N) with the input sequence length $L = 96$.

the highest possible value of 256. Figure 6 demonstrates the effectiveness of this expansion factor while keeping all other parameters fixed. With a higher state expansion factor, there is a certain chance of performance improvement for varying prediction lengths. Therefore, we set $N = 256$ as the default value for all datasets, and the results in Tables 2 and 3 contain the TimeMachine’s performance with this default value.

5.6 Ablation on Mamba Dimension Expansion Factor

We also experimented with the dimension expansion factor (E) of the Mambas, demonstrated in Supplementary Figure 3. Increasing the block expansion factor does not lead to consistent improvements in performance. Instead, higher expansion factors come with a heavy cost in memory and training time. Therefore, we set this value to 1 by default in all Mambas and report the results in Tables 2 and 3.

6 Conclusion

This paper introduces TimeMachine, a novel model that captures long-term dependencies in multivariate time series data while maintaining linear scalability and small memory footprints. By leveraging an integrated quadruple-Mamba architecture to predict with rich global and local contextual cues at multiple scales, TimeMachine unifies channel-mixing and channel-independence situations, enabling accurate long-term forecasting. Extensive experiments demonstrate the model’s superior performance in accuracy, scalability, and memory efficiency compared to state-of-the-art methods. Future work will explore TimeMachine’s application in a self-supervised learning setting.

Acknowledgements

This research is supported in part by the NSF under Grant IIS 2327113 and the NIH under Grants R21AG070909, P30AG072946, and R01HD101508-01.

We would thank the University of Kentucky Center for Computational Sciences and Information Technology Services Research Computing for their support and use of the Lipscomb Compute Cluster and associated research computing resources.

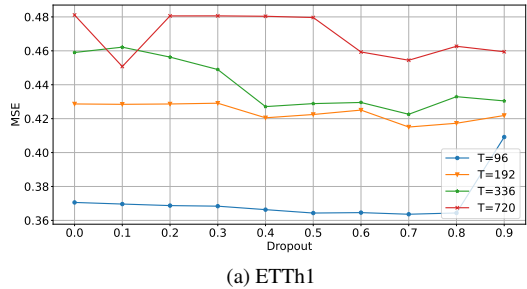
References

- [1] M. A. Ahamed and Q. Cheng. Mambatab: A simple yet effective approach for handling tabular data. *arXiv preprint arXiv:2401.08867*, 2024.
- [2] A. Ali, I. Zimerman, and L. Wolf. The hidden attention of mamba models. *arXiv preprint arXiv:2403.01590*, 2024.
- [3] A. Behrouz and F. Hashemi. Graph mamba: Towards learning on graphs with state space models. *arXiv preprint arXiv:2402.08678*, 2024.
- [4] R. Bommasani, D. A. Hudson, E. Adeli, R. Altman, S. Arora, S. von Arx, M. S. Bernstein, J. Bohg, A. Bosselut, E. Brunskill, et al. On the opportunities and risks of foundation models. *arXiv preprint arXiv:2108.07258*, 2021.
- [5] G. E. Box, G. M. Jenkins, G. C. Reinsel, and G. M. Ljung. *Time series analysis: forecasting and control*. John Wiley & Sons, 2015.
- [6] A. Das, W. Kong, A. Leach, S. K. Mathur, R. Sen, and R. Yu. Long-term forecasting with tiDE: Time-series dense encoder. *Transactions on Machine Learning Research*, 2023. ISSN 2835-8856. URL <https://openreview.net/forum?id=pCbC3aQB5W>.
- [7] E. Eldele, M. Ragab, Z. Chen, M. Wu, C. K. Kwok, X. Li, and C. Guan. Time-series representation learning via temporal and contextual contrasting. *arXiv preprint arXiv:2106.14112*, 2021.
- [8] S. Elfwing, E. Uchibe, and K. Doya. Sigmoid-weighted linear units for neural network function approximation in reinforcement learning. *Neural Networks*, 107:3–11, 2018. ISSN 0893-6080. doi: <https://doi.org/10.1016/j.neunet.2017.12.012>. URL <https://www.sciencedirect.com/science/article/pii/S0893608017302976>. Special issue on deep reinforcement learning.
- [9] J.-Y. Franceschi, A. Dieuleveut, and M. Jaggi. Unsupervised scalable representation learning for multivariate time series. *Advances in neural information processing systems*, 32, 2019.
- [10] D. Y. Fu, T. Dao, K. K. Saab, A. W. Thomas, A. Rudra, and C. Re. Hungry hungry hippos: Towards language modeling with state space models. In *International Conference on Learning Representations*, 2022.
- [11] A. Gu and T. Dao. Mamba: Linear-time sequence modeling with selective state spaces. *arXiv preprint arXiv:2312.00752*, 2023.
- [12] A. Gu, K. Goel, and C. Re. Efficiently modeling long sequences with structured state spaces. In *International Conference on Learning Representations*, 2021.
- [13] A. Gu, I. Johnson, K. Goel, K. Saab, T. Dao, A. Rudra, and C. Ré. Combining recurrent, convolutional, and continuous-time models with linear state space layers. *Advances in Neural Information Processing Systems*, 34:572–585, 2021.
- [14] K. He, X. Zhang, S. Ren, and J. Sun. Deep residual learning for image recognition. In *Proceedings of the IEEE conference on computer vision and pattern recognition*, pages 770–778, 2016.
- [15] S. Hochreiter and J. Schmidhuber. Long short-term memory. *Neural computation*, 9(8):1735–1780, 1997.
- [16] T. Kim, J. Kim, Y. Tae, C. Park, J.-H. Choi, and J. Choo. Reversible instance normalization for accurate time-series forecasting against distribution shift. In *International Conference on Learning Representations*, 2022. URL <https://openreview.net/forum?id=cGDAkQo1COp>.
- [17] D. P. Kingma and J. Ba. Adam: A method for stochastic optimization. *arXiv preprint arXiv:1412.6980*, 2014.
- [18] Z. Li, S. Qi, Y. Li, and Z. Xu. Revisiting long-term time series forecasting: An investigation on linear mapping. *arXiv preprint arXiv:2305.10721*, 2023.
- [19] M. Liu, A. Zeng, M. Chen, Z. Xu, Q. Lai, L. Ma, and Q. Xu. Scinet: Time series modeling and forecasting with sample convolution and interaction. *Advances in Neural Information Processing Systems*, 35: 5816–5828, 2022.
- [20] Y. Liu, H. Wu, J. Wang, and M. Long. Non-stationary transformers: Exploring the stationarity in time series forecasting. *Advances in Neural Information Processing Systems*, 35:9881–9893, 2022.
- [21] Y. Liu, T. Hu, H. Zhang, H. Wu, S. Wang, L. Ma, and M. Long. itransformer: Inverted transformers are effective for time series forecasting. In *The Twelfth International Conference on Learning Representations*, 2024. URL <https://openreview.net/forum?id=JePfAI8fah>.
- [22] J. Ma, F. Li, and B. Wang. U-mamba: Enhancing long-range dependency for biomedical image segmentation. *arXiv preprint arXiv:2401.04722*, 2024.
- [23] Y. Nie, N. H. Nguyen, P. Sinthong, and J. Kalagnanam. A time series is worth 64 words: Long-term forecasting with transformers. In *The Eleventh International Conference on Learning Representations*, 2023. URL <https://openreview.net/forum?id=Jbdc0vTOcol>.
- [24] A. Paszke, S. Gross, F. Massa, A. Lerer, J. Bradbury, G. Chanan, T. Killeen, Z. Lin, N. Gimelshein, L. Antiga, et al. Pytorch: An imperative style, high-performance deep learning library. *Advances in neural information processing systems*, 32, 2019.
- [25] Y. Schiff, C.-H. Kao, A. Gokaslan, T. Dao, A. Gu, and V. Kuleshov. Caduceus: Bi-directional equivariant long-range dna sequence modeling. *arXiv preprint arXiv:2403.03234*, 2024.
- [26] S. Tonekaboni, D. Eytan, and A. Goldenberg. Unsupervised representation learning for time series with temporal neighborhood coding. *arXiv preprint arXiv:2106.00750*, 2021.
- [27] P. Triarat, Y. Shin, J. Kang, Y. Nam, J. Na, M. Bae, J. Kim, B. Kim, and J.-G. Lee. Universal time-series representation learning: A survey. *arXiv preprint arXiv:2401.03717*, 2024.
- [28] A. Vaswani, N. Shazeer, N. Parmar, J. Uszkoreit, L. Jones, A. N. Gomez, Ł. Kaiser, and I. Polosukhin. Attention is all you need. *Advances in neural information processing systems*, 30, 2017.
- [29] H. Wu, J. Xu, J. Wang, and M. Long. Autoformer: Decomposition transformers with auto-correlation for long-term series forecasting. *Advances in neural information processing systems*, 34:22419–22430, 2021.
- [30] H. Wu, T. Hu, Y. Liu, H. Zhou, J. Wang, and M. Long. Timesnet: Temporal 2d-variation modeling for general time series analysis. In *The eleventh international conference on learning representations*, 2022.
- [31] L. Yang and S. Hong. Unsupervised time-series representation learning with iterative bilinear temporal-spectral fusion. In *International conference on machine learning*, pages 25038–25054. PMLR, 2022.
- [32] Z. Yue, Y. Wang, J. Duan, T. Yang, C. Huang, Y. Tong, and B. Xu. Ts2vec: Towards universal representation of time series. In *Proceedings of the AAAI Conference on Artificial Intelligence*, volume 36, pages 8980–8987, 2022.
- [33] A. Zeng, M. Chen, L. Zhang, and Q. Xu. Are transformers effective for time series forecasting? In *Proceedings of the AAAI conference on artificial intelligence*, volume 37, pages 11121–11128, 2023.
- [34] G. Zerveas, S. Jayaraman, D. Patel, A. Bhamidipaty, and C. Eickhoff. A transformer-based framework for multivariate time series representation learning. In *Proceedings of the 27th ACM SIGKDD conference on knowledge discovery & data mining*, pages 2114–2124, 2021.
- [35] Y. Zhang and J. Yan. Crossformer: Transformer utilizing cross-dimension dependency for multivariate time series forecasting. In *The eleventh international conference on learning representations*, 2022.
- [36] H. Zhou, S. Zhang, J. Peng, S. Zhang, J. Li, H. Xiong, and W. Zhang. Informer: Beyond efficient transformer for long sequence time-series forecasting. In *Proceedings of the AAAI conference on artificial intelligence*, volume 35, pages 11106–11115, 2021.
- [37] T. Zhou, Z. Ma, Q. Wen, X. Wang, L. Sun, and R. Jin. Fedformer: Frequency enhanced decomposed transformer for long-term series forecasting. In *International conference on machine learning*, pages 27268–27286. PMLR, 2022.

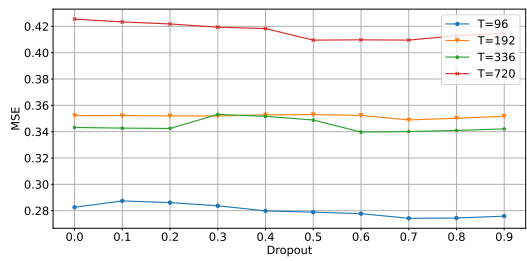
Supplementary Materials

Table 1: Ablation experiment on the residual connections with input sequence length $L = 96$ and $T = \{96, 192, 336, 720\}$.

Prediction (T) →		96		192		336		720	
\mathcal{D}	Res.	MSE	MAE	MSE	MAE	MSE	MAE	MSE	MAE
ETTh1	✗	0.366	0.395	0.423	0.425	0.430	0.427	0.474	0.462
	✓	0.364	0.387	0.415	0.416	0.429	0.421	0.458	0.453
ETTh2	✗	0.281	0.337	0.347	0.386	0.352	0.383	0.415	0.435
	✓	0.275	0.334	0.349	0.381	0.340	0.381	0.411	0.433



(a) ETTh1

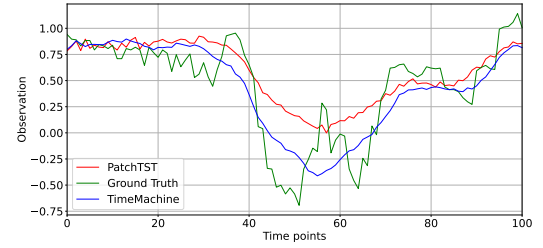


(b) ETTh2

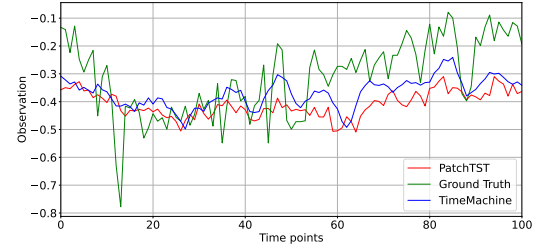
Figure 1: Performance (MSE) comparison concerning a diverse range of dropouts with input sequence length, $L = 96$.

Table 2: Results for the long-term forecasting task with varying input sequence length $L = \{192, 336, 720\}$ and $T = \{96, 192, 336, 720\}$

Prediction (T) →		96		192		336		720	
\mathcal{D}	L	MSE	MAE	MSE	MAE	MSE	MAE	MSE	MAE
Weather	192	0.155	0.204	0.198	0.243	0.241	0.281	0.327	0.336
	336	0.151	0.201	0.192	0.240	0.236	0.278	0.318	0.334
	720	0.151	0.203	0.195	0.246	0.239	0.285	0.321	0.340
ETTh1	192	0.365	0.386	0.415	0.413	0.406	0.417	0.447	0.459
	336	0.360	0.387	0.398	0.410	0.386	0.411	0.443	0.457
	720	0.363	0.395	0.402	0.418	0.396	0.420	0.468	0.476
ETTh2	192	0.274	0.334	0.340	0.379	0.327	0.378	0.402	0.432
	336	0.267	0.334	0.324	0.375	0.316	0.375	0.392	0.429
	720	0.260	0.332	0.314	0.372	0.316	0.377	0.394	0.433
ETTm1	192	0.286	0.337	0.331	0.365	0.354	0.384	0.421	0.421
	336	0.286	0.337	0.328	0.364	0.355	0.381	0.408	0.413
	720	0.289	0.344	0.334	0.369	0.357	0.382	0.416	0.413

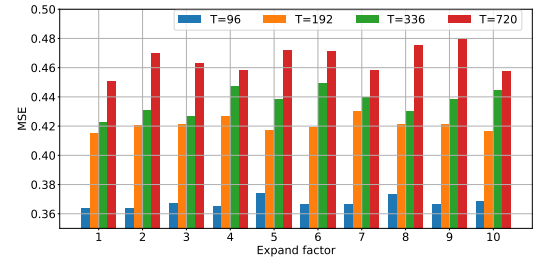


(a) ETTh1

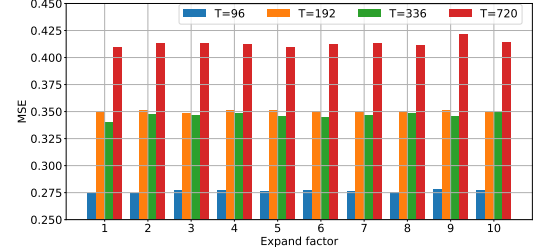


(b) ETTh2

Figure 2: Qualitative comparison between TimeMachine and second best-performing methods from Table 2. Observations are demonstrated from the test set for the case of $L = 96$ and $T = 720$ with a randomly selected channel and window frame of 100 time points.

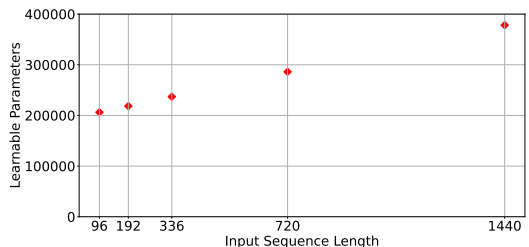


(a) ETTh1

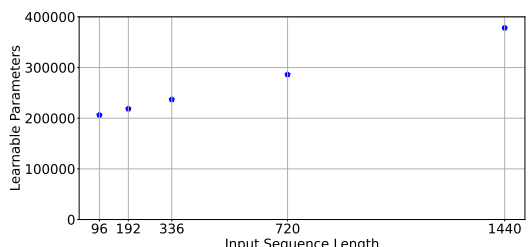


(b) ETTh2

Figure 3: Comparative analysis for the expanding factor.



(a) ETTh2



(b) Weather

Figure 4: Scalability in terms of learnable parameters with respect to look-back window.